

Application of Parametric Methods for Earthquake Precursors Using GPS TEC

R. Revathi, K. S. Ramesh, S. Koteswara Rao and K. Uday Kiran

Abstract Total Electron Content (TEC) perturbations observed for event happened on 15th January 2014 in Indonesia with the magnitude of $M \sim 4.5$ on Richter scale are investigated. The earthquake occurred at 9:26 h Greenwich Mean Time (GMT). Yule–Walker, Covariance, Modified Covariance and Burg parametric methods are used to find out the change in the spectrum of signals with and without disturbances in the signal. From the analysis, it is observed that ionosphere was disturbed thrice due to the impending earthquake resulting in upraise of energy in the ionosphere at 10:13 h LTC, 10:40 h LTC and finally at 10:52 h LTC, which is coinciding with that of the earthquake occurrence. These studies in future may help in developing early-warning systems for earthquakes.

Keywords Total electron content · Parametric methods · Earthquake

1 Introduction

The analysis of electromagnetic perturbations, prior to the occurrence of the earthquake, has often been considered to be a promising tool for their short-term prediction [1]. The seismogenic electromagnetic signals cover a wide range of frequencies from DC to VHF [4]. Even though the cause for the seismo-ionospheric perturbations is not yet clearly known, these disturbances have been established by

R. Revathi (✉) · K. S. Ramesh · S. Koteswara Rao · K. Uday Kiran
Department of ECE, KL University, Vaddeswaram, Guntur (DT)
522502, Andhra Pradesh, India
e-mail: revathimouni@gmail.com

K. S. Ramesh
e-mail: dr.ramesh@kluniversity.in

S. Koteswara Rao
e-mail: rao.sk9@gmail.com

K. Uday Kiran
e-mail: meemithrudu@gmail.com

many scientists statistically by removing the possible sources like solar flares, geomagnetic storm activity using running median values in Total Electron Content (TEC) [6].

Mechanical transformations with active geochemical processes are the most prevalent phenomena in the area of earthquake occurrence leading to the emanations of radon, noble gases. The radioactive emissions expend their energy in ionization and excitation of the elementary particles in the atmosphere [8]. The near ground plasma collides with the atmospheric constituents such as CO_2 , SO_x , NO_x , etc. leading to the generation of ions and free electrons, which quickly attach with the oxygen in a three-body reaction [2].

The free electrons attach to the metal atoms generating negative ions. The activated ions participate in ion-molecular reactions with the H_2O , which is present in large amount in troposphere. Thus, H_2O in the troposphere plays a major role in the formation of long living ions [3]. Hydrated ions including radon become centres of water condensations. During this process, latent heat is released and the atmosphere gets heated up resulting in convective activity of the ions. The substantial dipole moment of the water molecule $\mu = 1.87\text{D}$ prevents these molecules from recombination. Coulomb force of attraction results in the formation of positive, negative and quasi-neutral clusters.

Intense movements in air damage the neutral clusters due to weak Coulomb force of attraction. Thus, the atmosphere near ground becomes rich in long-living ion clusters. The different mobility of the ion clusters results in charge separation [7]. The increase in ion hydration reduces the columnar conductivity of the air column. The above-discussed charge clusters are assembled from about 4–5 m above the ground. These assembled clusters develop an electric field in surface near earth vertically [4, 5]. Thus, the anomalous vertical electric field acts as an electrical source, connecting the near earth surface and the upper atmosphere, leading to change in the upper atmosphere dynamo currents resulting in seismo-ionospheric perturbations.

Pulinets and Boyarchuk developed a simulation model for penetration of the anomalous vertical electric field. According to it, the value of the electric field changes with height, and it has a rapid initial increase at minimum and slow decay after reaching the maximum value. The penetration of the electrical field is larger at night-time than in day-time [6]. The existing lithosphere–atmosphere–ionosphere coupling mechanism is persistent with these changes [7].

Advancement in the technology of the Global Positioning Systems (GPS) paved a way to the study of seismo-ionosphere perturbations. The ionosphere being a dispersive medium causes a delay in electromagnetic signals passing through ionosphere. The time delay is calculated by using principal of ‘time of arrival’.

The ground-based GPS receiver calculates the Slant Total Electron Content (STEC) which is defined as the integral no. of electrons present in line of sight path from satellite to receiver. The change in speed of the GPS signal travelling through ionosphere leads to the change in the signal transit time due to the changes in refractive index of medium. The pseudorange in metres for GPS receiver of single frequency ‘ ρ_{L_1} ’ is given by

$$\rho_{L_1} = (40.3 * \text{STEC}) / f_{L_1}^2 \quad (1)$$

For GPS receivers with two frequencies

$$\rho_{L_1} - \rho_{L_2} = (40.3 * \text{STEC}) * [(1/f_1^2) - (1/f_2^2)] \quad (2)$$

where f_1 and f_2 correspond to frequencies of GPS L_1 and L_2 signals. STEC for GPS receiver with two frequencies is

$$\text{STEC} = (1/40.3) * [(f_{L_1}^2 * f_{L_2}^2) / (f_{L_1}^2 - f_{L_2}^2)] * (\rho_{L_1} - \rho_{L_2}) \quad (3)$$

The STEC values change with the movement of the satellite. At a particular time, many satellites are seen by the ground-based receiver. Vertical Total Electron Content (VTEC(V)) is calculated by

$$V = \text{STEC} * \cos(\xi) \quad (4)$$

where $\xi' = 90^\circ$ —satellite zenith angle at ionospheric pierce point. Generally, it is considered to be a height of 350 km from the surface of the earth [8]. The anomaly detection of seismo-ionospheric perturbations is carried on GPS TEC data on global scale (GIM data, GDGPS and NASA's data) [9–11]. Global scale TEC values are taken from a group of GPS receivers.

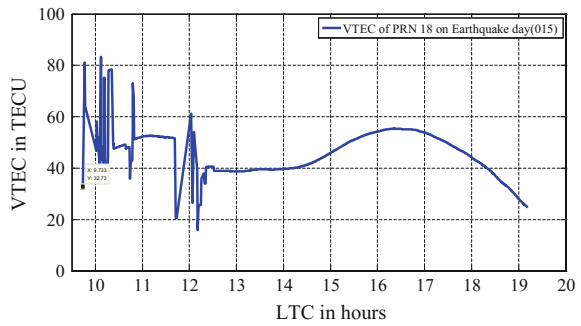
The demerits in analysing seismo-ionospheric perturbations using a network of ground-based GPS receivers (global TEC data) are as follows. 1. The global TEC data includes modelling errors, and it may not be possible to study the specific phenomena leading to the occurrence of earthquake. 2. A network of GPS stations, where all receivers are not situated in a particular geometry, estimation of TEC values for points nearer and farther distances leads to validation of the data at a specific point in the upper atmosphere. 3. The global TEC data used in the analysis has different sampling times. For example, the sampling period for EURF network situated in Italy is 2.5 min, and Global Ionospheric Maps (GIM) data has a sampling period of 2 h, etc.

Implementation of signal processing algorithms results in accurate signal estimation. Parametric methods are helpful in identification of underlying stationary signal structure, described by using a limited number of parameters. These methods are useful in detecting and tracking changes in the data set. In this paper, Autoregressive AR(4) methods are used for anomaly detection regarding earthquakes. Yule–Walker, Burg, Covariance and Modified Covariance are used for the analysis. The analysis is carried out for the catastrophic event occurred on 15th January 2014 in Indonesia (6.33° S, 106.896° E) at 9:56 h, Greenwich Mean Time with a depth of 125 km.

Fig. 1 Location map of the earthquake



Fig. 2 VTEC plot of satellite PRN 18



2 Data

GPS VTEC is staked by the International GNSS Service (IGS). It is noticed that the VTEC of satellite 18 is perturbed on the earthquake day. The location map of the earthquake is shown in Fig. 1, taken from <http://earthquaketrack.com/quakes/2014-01-15-09-26-11-utc-4-5-125>, and the VTEC plot of satellite 18 is shown in Fig. 2.

3 Methodology

Parametric methods use the knowledge of data generation in the estimation procedure. The investigation was carried out using fourth-order Autoregressive (AR (4)) models [12, 13].

Yule–Walker, Covariance, Modified Covariance and Burg algorithms are synthesized, and their respective normalized frequencies are 0.2002 and 0.298. Power Spectral Density (PSD) of Yule–Walker is different from the remaining PSDs. It does not effectively represent the frequencies present in the data. PSDs of Covariance and Modified Covariance are scaled so as to clearly represent them in

Fig. 3 PSD's of Yule–Walker, Covariance, Modified Covariance and Burg methods for the synthetic signal

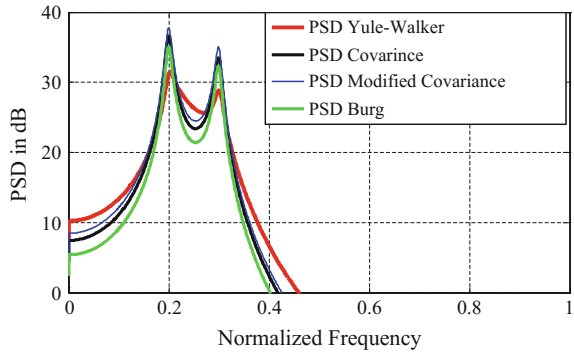


Fig. 4 Detrended R_1 data

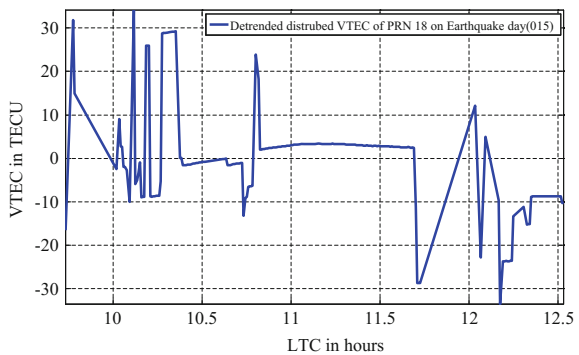


Fig. 3. Burg PSD has predominantly represented the normalized frequencies in the data. After the implementation of the algorithms on the synthetic signal these are applied on the disturbed and undisturbed VTEC for identification of earthquake precursors.

The TEC perturbation in satellite number 18 is not available before occurrence time of the disturbance, and it is divided into disturbed and undisturbed parts on the earthquake day. The diurnal and seasonal variations in VTEC are removed by detrending the data. The detrended disturbed (R_1) and undisturbed (R_2) data sets are

Fig. 5 Detrended R_2

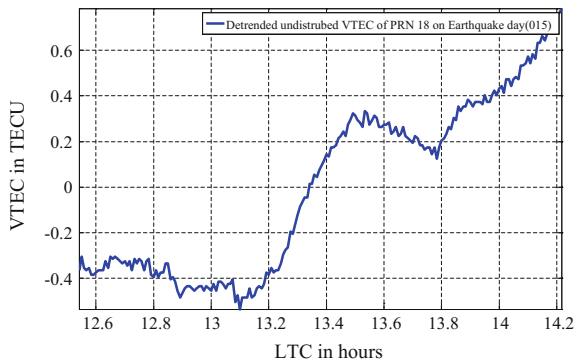


Fig. 6 PSD of disturbed VTEC for all four methods

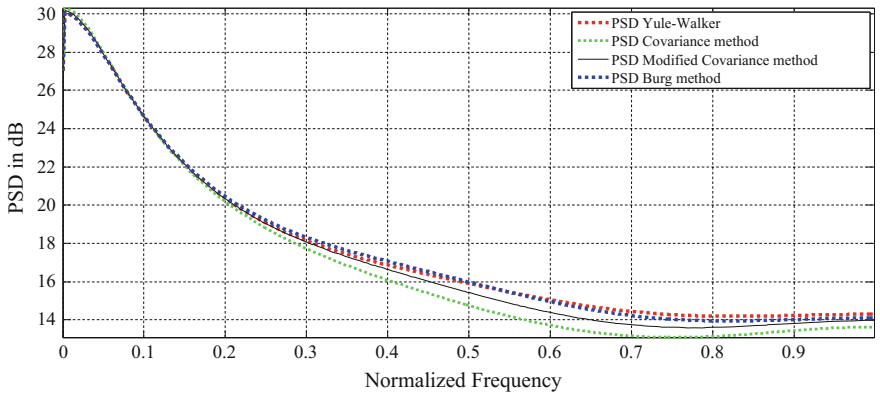
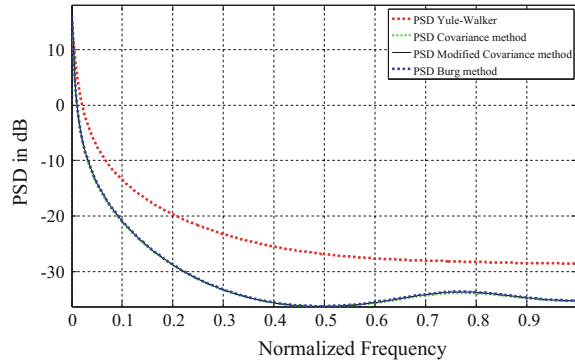


Fig. 7 PSD of undisturbed VTEC for all four methods

represented in Figs. 4 and 5. The TEC data of PRN 18 consists of 1042 points. R_1 and R_2 segments of data consist of 240 and 202 data points, respectively. The methods are applied on both R_1 and R_2 sets to identify the underlying salient features of non-stationary TEC data.

It is observed that the PSD of R_1 data has significant positive value (14 dB) when compared to that of the undisturbed data. PSD plots characterize the energy in the ionosphere due to impending earthquake. PSDs of above methods for both R_1 and R_2 sets are shown in Figs. 6 and 7. Among the four spectrum estimation methods applied on GPS VTEC, Burg method has given better results. The PSDs of R_1 and R_2 sets are given in Table 1 (Fig. 8).

The disturbed VTEC data segment is subjected to multi-resolution analysis to identify earthquake precursors. Burg algorithm is implemented on those segments of data to understand the conjuncture of earthquake on the ionosphere. The first bisection of disturbed data segment resulted in upraise of energy at normalized

Table 1 PSD of the disturbed and undisturbed data using Yule–Walker, Covariance, Modified Covariance and Burg methods

S. No	Method	Disturbed approx. range (dB)	Undisturbed approx. range (dB)
1	Yule–Walker	14.19	−28.22
2	Covariance	13.19	−28.22
3	Modified Covariance	13.64	−33.64
4	Burg	13.95	−33.64

Fig. 8 PSD of R_1 for 120 points each

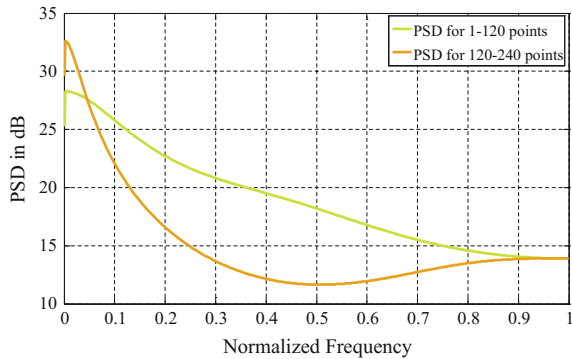
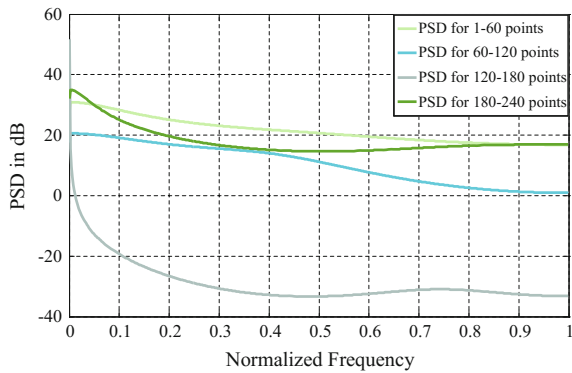


Fig. 9 PSD of R_1 for 60 points each



frequencies 0.9247 with PSD 13.98 dB in the second data segment. The PSD plot of two segments of R_1 of 120 points is shown in Fig. 9.

As spectral resolution increases, certainty in time of occurrence of perturbations in VTEC also increases. So R_1 is bisected into segments of 60, 30 and 15 points each. Application of Burg algorithm on second bisection of the data resulted in a small peak in the third segment of the data. Figure 10 represents the PSD for data segments of 60 data points each. Further, R_1 is sampled into sets of 30 and 15

Fig. 10 PSDs of R_1 for first four sets with 30 points

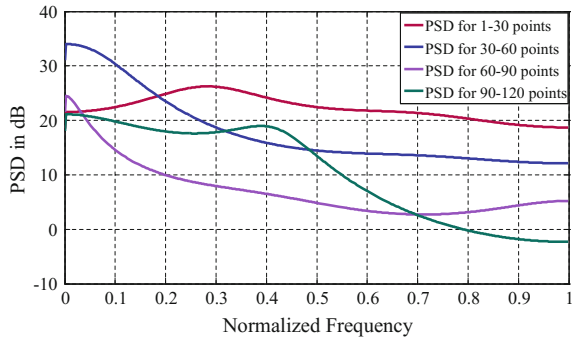
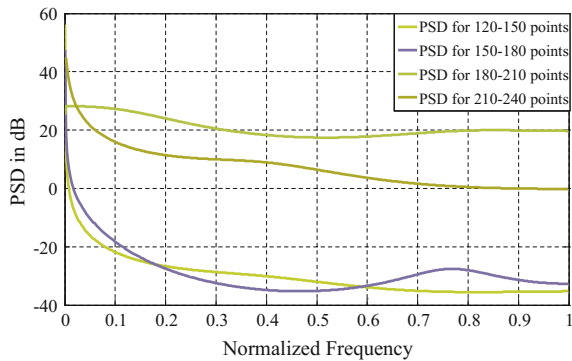


Fig. 11 PSDs for second four sets of R_1 with 30 points



points to notice the clear upraise in the disturbance. In first and fourth sets of 30 points, peaks are identified at normalized frequencies of 0.2815 and 0.4066 with PSDs of 26.24 dB and 18.83 dB, respectively. In the third and the second sets, the energy is abating.

A peak is again seen in the sixth set with a normalized frequency of 0.7742 with a PSD of -27.62 dB. The PSDs for disturbed data sets with 30 points each are given in Fig. 11. The PSDs were also drawn for data frames of 15 points each. The PSDs of data with 15 points each are shown in Figs. 12 and 13. It is clearly observed from Fig. 12 that first, third and fourth data sets have peaks at a normalized frequency of 0.6432, 0.2893 and 0.6197 with a PSDs of 27.03 dB, 29.01 dB and -28 dB.

In the fifth to eight data sets containing 15 points, it is observed that the energy has abated in the seventh set. In the eighth set, a peak is observed at normalized frequency of 0.6315 with a PSD of -28.83 dB. In the remaining sets of data with 15 points, each no significant change had been noticed. From the analysis, it is clearly identified that the ionosphere is disturbed thrice at 10:13 h LTC, 10:40 h LTC and finally at 10:52 h LTC. As the GPS receiver is located near to the epicentre (58 km), these perturbations may be considered to represent the impending earthquake.

Fig. 12 PSDs for first four sets of R_1 with 15 points

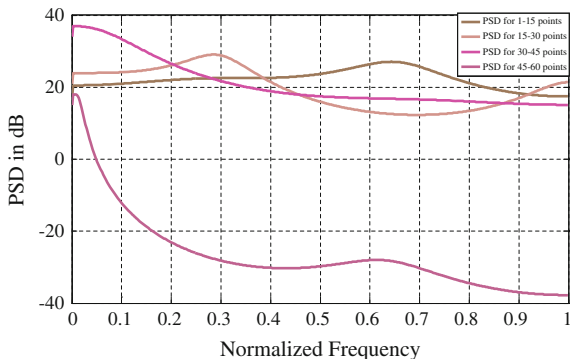
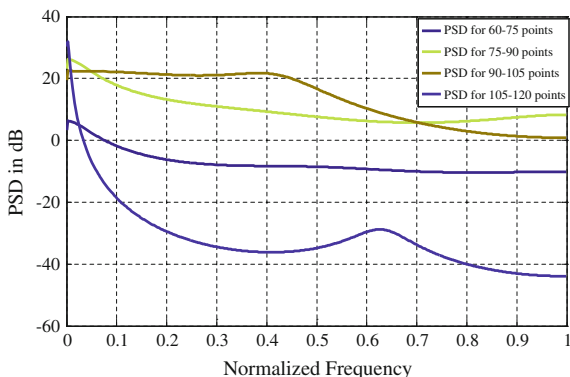


Fig. 13 PSDs for second four sets of R_1 with 15 points



4 Conclusion

Anomalies in GPS VTEC on the earthquake day clearly show that use of Burg algorithm could recognize co-seismic disturbances in ionosphere. From the analysis, the ionosphere is disturbed thrice at 10:13 h LTC, 10:40 h LTC and finally at 10:52 h LTC. According to the available literature, the ionosphere is disturbed few days before the earthquake. In this analysis, we can also identify the latitude and longitude of these perturbations. A thorough analysis of GPS VTEC for seismo-ionospheric perturbations using spectrum estimation methods, ahead of the occurrence, may lead to identification of possible precursors of earthquakes in ionosphere. In future, these studies may be used for the development of early-warning systems for earthquakes.

Acknowledgements Author’s sincere acknowledgments are given to DST, Government of India for finically funding this work under the projects SR/AS-04/WOS-A/2011 and SR/S4/AS-91/2012.

References

1. Su, Y.C., et al.: Temporal and spatial precursors in ionospheric total electron content of the 16 October 1999 Mw7.1 hector mine earthquake. *J. Geophys. Res. Space Phys.* **118**, 6511–6517. <https://doi.org/10.1002/jgra.50586> (2013)
2. Pulinets, S.: Ionospheric precursors of earthquakes; recent advances in theory and practical applications. *TAO* **15**(3), 413–435 (2004)
3. Singh, A.K., et al.: Electrodynamical coupling of earth's atmosphere and ionosphere: an overview. *Int. J. Geophys.* **2011**, Article ID 971302, 13 pages. <https://doi.org/10.1155/2011/971302>
4. Lin, J.W.: Ionospheric total electron content (TEC) anomalies associated with earth quakes through Karhunen-Loève trans form (KLT). *Terr. Atmos. Ocean. Sci.* **21**(2), 253–265 (2010)
5. Gosh, D., Midy, S.K.: Associating an ionospheric parameter with major earthquake occurrence throughout the world. *J. Earth Syst. Sci.* **123**(1), 63–71
6. Boyarchuk, K.A.: Estimation of the concentration of complex negative ions resulting from radioactive contamination of the troposphere. *Tech. Phys.* **44**(3)
7. Pulinets, S.A., Boyarchuk, K.A.: *Ionospheric Precursors of Earthquakes*. Springer Publ (2004)
8. Mishra, P.: *Global Positioning Systems*, 2nd edn. Ganga-Jamuna Press
9. Molchanov, O., et al.: lithosphere-atmosphere-ionosphere coupling as governing mechanism for pre-seismic short term events in atmosphere and ionosphere. *Natural Hazards Earth Syst. Sci.* **4**, 757–767 (2004)
10. Lin, J.W.: Ionospheric precursor for the 20 April, 2013, Mw = 6.6 China' Lushan earthquake: two-dimensional principal component analysis (2DPCA). *German J. Earth Sci. Res. (GJESR)*, **1**(1), 1–12 (2013)
11. Contadakis, M.E., et al.: TEC variations over the mediterranean during the seismic activity period of the last quarter of 2005 in the area of Greece. *Nat. Hazards Earth Sys.* **8**, 1267–1276
12. Hayes M.H.: *Statistical digital processing and modeling*. Georgia Institute of Technology, Wiley, Inc
13. Revathi, R., Lakshminarayana, S., Koteswara Rao, S., Ramesh, K.S., Uday Kiran, K.: Observation of ionospheric disturbances for earthquakes ($M > 4$) occurred during june 2013 to july 2014 in Indonesia using wavelets. *Proc. SPIE* **9876**, 98763E. © 2016 SPIE · CCC code: 0277-786X/16/\$18 · <https://doi.org/10.1117/12.2227301>